

Supplementary Materials

Materials and Methods

Reagents. Antibodies were purchased from the following companies. Abcam: anti-WRN (ab200), anti-NANOG (ab21624), anti-H3K9me3 (ab8898), anti-Laminin (ab11575); Santa Cruz Biotechnology: anti-WRN (SC-5629), anti-OCT4 (SC-5279), anti-SOX2 (SC-17320), anti- β -actin (SC-130301), anti-TRA-1-81 (SC-21706), anti-LBR (SC-160482), anti-Myc (SC-41), anti-GFAP (SC-9065); Cell Signaling: Phospho-(Ser/Thr) ATM/ATR Substrate Antibody (2851), anti-HP1 α (2616); Millipore: anti- γ -H2AX (05-636), anti-SUV39H1 (05-615), anti-human Lamin A/C (MAB3211); Sigma: anti-SMA (A5228), anti-AFP (A8452); BD Bioscience: anti-LAP2 β (611000), anti-CD34 (555822), anti-CD43 (560198), anti-CD45 (555482), anti-CD73 (550741), anti-CD90 (555595); Bethyl Laboratories: anti-53BP1 (A300-273A); Vector: anti-Ki67 (VP-RM04); eBioscience: anti-CD105 (17-1057). All chemicals were purchased from Sigma. Lentiviral WRN vector, YFP-WRN, and HP1 α -Myc were kindly provided by Dr. Lucio Comai, Dr. Michel Lebel, and Dr. Weiguo Zhu, respectively (21-23).

Cell culture. H9 and H1 ESCs (WiCell Research) and their WRN or SUV39H1-mutant derivatives were maintained on Mitomycin C treated mouse embryonic fibroblasts (MEFs) in human ESC medium or on Matrigel (BD Biosciences) coated plates in mTeSR medium (STEMCELL Technology). The ESC medium contains DMEM/F12 (Invitrogen) supplemented with 20% Knockout Serum Replacement (Invitrogen), 0.1 mM non-essential amino acids (NEAA, Invitrogen), 2 mM GlutaMAX (Invitrogen), 55 μ M β -mercaptoethanol (Invitrogen), and 10 ng/ml bFGF (Joint Protein Central). Wild type, WRN knockout, SUV39H1^{H324K} MSC, and human dental pulp-derived primary MSCs were maintained in α MEM medium (invitrogen) with 10% fetal bovine serum (FBS, Hyclone), 1% penicillin/streptomycin (Gibco), 10 ng/ml bFGF (JPC). HEK 293T cells were maintained in high glucose DMEM containing 10% FBS.

HDAdV preparation. WRN-HDAdV for gene knockout was generated using a BAC clone containing the human WRN locus (RP11-473A17, BACPAC Resources), which was modified using BAC recombination (24). In brief, an FRT-PGK-EM7-neo-bpA-FRT fragment was recombined into intron 14-16 of WRN in the BAC clone. A total of 21.2 kb of WRN homology sequence, including the marker cassette, was subcloned into the HDAdV plasmid pCIHDAdGT8-4 (kindly provided by Dr. Kohnosuke Mitani) (25). SUV39H1^{H324K}-HDAdV for mutation knock-in was generated using a BAC clone containing the human SUV39H1 locus (RP11-1148L6, BACPAC Resources). In brief, intron 3-5 of SUV39H1 was PCR-amplified from RP11-1148L6 BAC DNA and subcloned into the pCR2.1-TOPO vector (Invitrogen). The H324K (CAC>AAA) mutation at exon 4 was introduced with 2 primers (SUV-mutation-P1 and SUV-mutation-P2, Table S5) using the GeneTailor Site-Directed Mutagenesis System (Invitrogen). An

FRT-PGK-EM7-neo-bpA-*FRT* fragment was subcloned into a site 753 bp upstream of exon 4 in the H324K mutated plasmid, and the generated DNA fragment was recombined into RP11-1148L6 BAC DNA using BAC recombineering. A total of 22.8 kb of *SUV39H1* homology, including the H324K mutation and marker cassette, was subcloned into the HDAdV plasmid pAMHDAdGT8-4. The generated *WRN*-HDAdV and *SUV39H1*^{H324K}-HDAdV plasmids were linearized by *PI-SceI* (NEB) and transfected into 116 cells (kindly provided by Dr. Philip Ng) in the presence of helper virus AdHPBGF35 (kindly provided by Dr. André M. Lieber) (26, 27). Crude virus extracts were serially amplified in 116 cells and then purified according to a previously described method (26). β -gal-transducing units (btu) were determined in 293 cells to define infectious vector titers.

Isolation of *WRN* gene knockout and *SUV39H1*^{H324K} knock-in human ESC clones. For generation of heterozygous *WRN* knockout ESCs, H9 human ESCs were infected with *WRN*-HDAdV at multiplicity of infection (MOI) 3-30 btu/cell. Two days after infection, G418 (100 μ g/ml; Invitrogen) was added to the medium to start positive selection. After 10-12 days, 4 μ M Ganciclovir (GANC; Invitrogen), in addition to G418, was added to the medium for negative selection. After additional 7-9 days, G418/GANC double-resistant clones were transferred to 96-well plates and expanded for further characterization. Gene-targeted clones were determined by PCR of genomic DNA from drug-resistant clones with the primers indicated in Figure S1A (Table S5) using LA Taq DNA Polymerase (TAKARA). Long PCR cycling included a 1 min initial denaturation at 94 $^{\circ}$ C, 14 cycles of 10 sec denaturation at 98 $^{\circ}$ C and a 10 min annealing and extension at 68 $^{\circ}$ C, 21 cycles of 10 sec denaturation at 98 $^{\circ}$ C and a 10 min plus 5 sec/cycle annealing and extension at 68 $^{\circ}$ C, plus a final extension at 68 $^{\circ}$ C for 10 min. For generation of heterozygous *WRN* knockout ESCs, we first removed the neomycin-resistance cassette from the targeted locus using a pCAG-Flpo-2A-puro vector as previously described (28). Removal of the neomycin-resistance cassette was verified by PCR using LA Taq Hot Start Version (TAKARA) and DNA sequencing with the primer WRN15/16-TOPO-F and WRN15/16-TOPO-R (Table S5). For generation of homozygous *WRN* knockout ESCs, the same targeting strategy was repeated in neomycin cassette-removed heterozygous *WRN* knockout cells. For generation of *SUV39H1*^{H324K} mutation knock-in hESCs, 3X 10⁶ feeder-free cultured H1 hESCs were dissociated by TrypLE, and resuspended in 1 ml MEF-conditioned medium containing 10 μ M Y-27632. Cells were infected with *SUV39H1*^{H324K}-HDAdV at MOI of 0.3-10 btu/cell at 37 $^{\circ}$ C for 1 h, and after brief centrifugation resuspended in 10 ml MEF-conditioned medium containing 10 μ M Y-27632. Cells were plated onto 100 mm dishes precoated with 1 x 10⁶ irradiated neomycin-resistant MEFs. Two days after infection, G418 (100 μ g/ml) was added to the medium to start positive selection. After 12 days, GANC (2 μ M) in addition to G418 was added to the medium to start negative selection. After an additional 7 days, G418/GANC double-resistant clones were transferred to 96-well plates and expanded for further characterization. Gene-targeting efficiency was determined by

PCR of genomic DNA from drug-resistant clones with the primers SUV-P1 to P4 (Table S5) using LA Taq Hot Start Version and long PCR cycling as described above. To determine mutation knock-in events, genomic DNA was extracted from the gene-targeted clones. Exon 4 of *SUV39H1* was PCR-amplified with SUV-P3 and SUV-P5 using LA Taq Hot Start Version. Amplicons were sequenced with an ABI 3730 sequencer (Applied Biosystems).

Generation and characterization of MSCs. Differentiation of wild type, *WRN* knockout, and *SUV39H1*^{H324K} ESC lines to mesenchymal stem cells (MSCs) was performed as described previously (29). In brief, groups of 10-14 EBs were plated on matrigel-coated 6-well plates in α MEM medium (invitrogen) with 10% fetal bovine serum (FBS, Hyclone), 1% penicillin/streptomycin (Gibco), 10 ng/ml bFGF (JPC), and 5 ng/ml TGF β (Humanzyme). Cells were left for about 10 days until differentiation to confluent fibroblast-like populations occurred. The resulting MSC-like cells were passaged once and then analyzed and sorted by FACS using various antibodies related to the MSC signature. The cells right after sorting were recorded as passage 0 (P0). Additionally, cells were stained with antibodies against CD73, CD90, and CD105. To demonstrate MSC integrity, cells were further differentiated towards bone, cartilage and adipose cells. To evaluate the differentiation capacity to osteogenic fate, MSCs were plated in osteogenic media [α MEM (Invitrogen) with 10% FBS, 1% penicillin/streptomycin, 10 mM β -glycerophosphate (Sigma), 0.2 mM ascorbate-2-phosphate (Sigma), and 0.1 μ M dexamethasone (Sigma)]. Similarly, in order to evaluate chondrogenic differentiation, pellets of 200,000 MSCs were suspended in chondrogenic media [DMEM-high glucose (Invitrogen) with 1% penicillin/streptomycin, 10 ng/ml TGF- β 1 (R&D Systems), 1x ITS (Sigma), 40 μ g/ml proline (Sigma), 50 μ g/ml ascorbate-2-phosphate (Sigma), and 0.1 μ M dexamethasone (Sigma)]. Adipogenic differentiation from MSCs was performed according to previous publications (29, 30). PPAR γ was used to facilitate adipogenesis (30). Differentiation protocols were maintained for approximately 21 days. Histochemical staining with von Kossa (osteogenic), Toluidine blue O (chondrogenic), and Oil red O (adipogenic), was conducted for differentiation analyses (31, 32).

Isolation and culture of human dental pulp-derived MSCs. Approval for the use of dental samples from human subjects was obtained from the ethics committee of 306 hospital of PLA in Beijing. Discarded teeth were freshly collected from healthy individuals of different ages. Primary MSCs from dental pulps were isolated as previously described (33, 34). Briefly, pulp tissue was removed from the teeth, minced, digested, and cultured in primary medium composed of α MEM medium with 10% FBS and 1 ng/ml bFGF. MSCs could outgrow the tissue and were cultured to passage 4 for further analysis. The sample information was described in Table S4.

Virus preparation. For lentiviral vectors expressing shRNA targeting *WRN*, *SUV39H1*, *LAP2 β* and *HP1 α* ,

corresponding shRNA oligo-nucleotides (Table S5) were inserted into the cloning site of pLVTHM/GFP (Addgene, 12247) that had been cleaved by the restriction endonucleases ClaI and MluI. For lentiviral vector encoding HP1 α -Myc, corresponding cDNA was amplified by PCR (Primers in Table S5) and cloned into pLE4 lentiviral vector (a gift from Dr. Tomoaki Hishida). For lentivirus packaging, HEK 293T were co-transfected with lentiviral vectors and packaging plasmids (psPAX2 (Addgene, 12260) and pMD2.G (Addgene, 12259)) using Lipofectamine 2000 (Invitrogen). Lentivirus particles were collected on day 2 and concentrated by ultracentrifugation at 19,400 g for 2.5 h.

Protein and mRNA analysis. For immunoblotting, cells were lysed in ice-cold lysis buffer as previously reported (28). Protein quantification was performed with a BCA kit (Thermo Fisher Scientific). 20 μ g of protein lysate was subjected to NuPAGE[®] Novex 3-8% Tris-Acetate Gel (Invitrogen) or 4-12% Bis-Tris gel and electrotransferred to a PVDF membrane (Millipore). Primary antibodies and HRP conjugated secondary antibodies (Jackson ImmunoResearch Labs) were incubated with the membrane sequentially. Protein expression was detected by Pierce ECL western blotting substrate kit (Pierce). The quantification of western blot was done by Image Lab software for ChemiDoc XRS system (Bio-Rad). For quantitative PCR, total RNA was extracted by TRIzol (Invitrogen), followed by cDNA synthesis with the GoScript[™] Reverse Transcription System (Promega). Genomic DNA was removed using the DNA-free[™] Kit from Ambion. Quantitative RT-PCR was performed using iTaq[™] Universal SYBR[®] Green Supermix (Bio-Rad). Sub-cloning was performed with PrimeSTAR (TAKARA) and the pEasy-blunt ligation kit (TransGen Biotech). Primer sequences are listed in Table S5.

Co-immunoprecipitation. Experiments were performed as previously described (22). WRN immunoprecipitation used CHAPS lysis buffer [40 mM HEPES pH7.5, 120 mM NaCl, 0.3% CHAPS, 1 mM EDTA, complete protease inhibitor cocktail (Roche)]. SUV39H1 and Myc-HP1 α immunoprecipitation used NP40 lysis buffer [1% NP40, 150 mM NaCl₂, 10% glycerol, 1 mM EDTA, 1mM EGTA, 20 mM Tris-Hcl (PH=7.5), complete protease inhibitor cocktail (Roche)]. In some cases, the protein inputs were prepared by directly lysing cells with SDS-sampling buffer. The proteins in the immunoprecipitates and inputs were analyzed by immunoblotting with specific antibodies.

Microscopy. For immunofluorescence microscopy, cells were fixed for 20 min in 4 % formaldehyde in PBS at room temperature. Subsequently, samples were permeabilized with 0.3% Triton X-100 in PBS at room temperature (RT) for 10 min. Cells were blocked with 10% donkey serum (Jackson ImmunoResearch Labs) in PBS for 1 h, and then incubated at 4 °C overnight with primary antibodies. Cells were washed three times in PBS and incubated at RT for 1 h with the corresponding secondary antibody (Invitrogen). DNA was stained with Hoechst 33342 (Invitrogen, 5 μ g/ml), and F-actin was stained with phalloidin (Invitrogen). For 3D fluorescence in situ hybridization (3D-FISH), cells were fixed in 4% formaldehyde for 10 min at RT, permeabilized with 0.5% Triton X-100 and stained with primary antibody

at 4 °C overnight. After repeated freezing in liquid nitrogen, hybridization was carried out overnight at RT with Cy3-labeled 100 nM centromere PNA probe (Panagene). Post-hybridization washes were carried out in 0.1X SSC at 60 °C. Samples were stained with biotin-labeled secondary antibody (Vector) and Alexa Fluor 488 conjugated streptavidin (Invitrogen), followed by counterstaining with Hoechst. We used Leica SP5 confocal for immunofluorescence microscopy, with the acquisition parameters set the same for each experiment. Quantitative microscopy was performed using around 100 randomly selected cells from each sample. Coefficient of Variation (C.V) of DNA texture image was used to measure the degree of variation of all pixel value in one nucleus, calculated by the formula ($C.V = \text{Standard deviation} / \text{Mean}$) with ImageJ. Electron Microscopy was performed according to previously protocols (35).

Flow cytometry analysis. For measurement of cell cycle, Click-iT® EdU Alexa Fluor® 647 Flow Cytometry Assay Kit (Invitrogen) was used according to the protocol. For measurement of TRA1-81 expression, cells were washed with PBS and incubated with primary antibody at 4 °C for 1 h, followed by secondary antibody incubation at 4 °C for 30 min. Alternatively, cells were treated with primary antibody conjugated with fluorescence dye. After washing, protein expression was measured using LSRFortessa™ cell analyzer (BD). Data were analyzed by FlowJo software.

Growth curve assay. Cell population doubling was determined as previously described (28). Growth rate of SUV39H1^{H324K} knock-in MSCs was monitored by Incucyte Zoom (Essen Bioscience) according to the instructions.

SA-β-gal staining. Staining was performed as described previously (36). Briefly, cultured cells were washed in PBS and fixed at RT for 3 min in 2% formaldehyde and 0.2% glutaraldehyde. Fixed cells were stained with fresh staining solution for SA-β-galactosidase activity at 37 °C overnight. The percentage of cells positive for SA-β-Gal staining were quantified and statistically analyzed.

ELISAs. ELISA kits to detect IL-6 (D6050) and IL-8 (D8000C) were purchased from R&D Systems, and used as previously reported (37). All ELISA data were normalized to cell number.

In vivo luminescence measurements. 100 μl of 1X10⁶ MSCs transduced with lentivirus expressing luciferase were injected into the midportion of the tibialis anterior (TA) muscle. 7 and 21 days after transplantation, mice were anaesthetized and treated with D-luciferin. Then, photon emission was measured by IVIS lumina system (PerkinElmer). Bioluminescence images were acquired for 50 second with f/stop=1 and binning=16. Photons were counted according to the digital false-color photon emission image of the mouse, and the values were normalized by average cellular luciferase intensity before transplantation

Teratoma analysis. To test the pluripotency *in vivo*, teratoma formation was assessed following injection of ESCs into

NOD-SCID mice. In short, 1×10^6 H9 ESCs, *WRN* deficient, or *SUV39HI*^{H324K} ESCs were injected subcutaneously into anaesthetized mice. Animals were sacrificed approximately 12 weeks after injection when teratoma formation was observed. All murine experiments were conducted in compliance with animal protocols approved by the Chinese Academy of Science Institutional Animal Care and Use Committee.

Karyotyping analysis. Standard G-Banding chromosome analysis was performed according to the previously published protocol (28).

Telomeric repeat amplification protocol (TRAP) and telomere length measurement. TRAP was performed to assess telomerase activity using commercially available kit (Millipore, S7700). 36-bp band in every lane was served as internal control to calculate the relative telomerase activity of each sample according to manufactory's instruction. Telomere length was determined by a quantitative PCR-based method with $n=8$, as established previously (38).

Whole genome sequencing library construction. Genomic DNA was isolated from cells using the DNeasy Blood & Tissue Kit (Qiagen) according to the manufacturer's protocol. Followed by shearing 1-2 μg of DNA into an average size of 200 bp and purifying with a QIAquick PCR Purification kit (Qiagen). Sequencing library construction was performed with a TruSeq DNA Sample Preparation Kit (Illumina) according to the manufacturer's standard manual.

Analysis of copy number variations (CNVs). First, the low quality sequences and adapter sequences were filtered and removed from the raw reads. Then, the remaining reads were aligned to the human reference genome (hg19 from UCSC) by BWA. Normalized number of the reads per non-N window of 500 kb were calculated by the following formula, $C = d * m * 10^4 / ((m-t) * td)$, in which d is the number of mapped bases located in the 500 kb widow, m is the window size, t is the number of N in the hg19 reference genome in the window, td is the total number of bases mapped to the genome. CNVs that changed over 40% in late passage MSCs-*WRN*^{-/-} compared with early passage MSCs-*WRN*^{-/-} were taken into account.

Chromatin immunoprecipitation (ChIP) and deep sequencing. We performed ChIP-seq according to a previous protocol with minor modifications (39). One million cells per sample were cross-linked by 1% vol/vol formaldehyde for 8 or 15 minutes at room temperature. Samples were then re-suspended in lysis buffer (50 mM Tris-HCl, 10 mM EDTA, 1% SDS, pH8.0) for 5 min on ice. Subsequently, lysates were sonicated using a Covaris S2 instrument. The fragmented chromatins were incubated overnight with Protein A-bead bound with 2.4 μg or 5 μg antibody as following: anti-H3K4me3 (Abcam, ab8580), anti-H3K27me3 (CST, 9733), anti-H3K9me3 (Abcam, ab8898), anti-*WRN* (Abcam, ab200). Normal rabbit IgG (Santa Cruz, SC-2027) or input served as a control. Chromatin of interest was eluted in elution buffer (20 mM Tris-HCl, 5 mM EDTA, 50 mM NaCl, pH7.5). Next the chromatin was digested and

de-cross-linked with Proteinase K by incubation at 68 °C for 2 h on a thermomixer at 1,300 rpm. Then the DNA was isolated using phenol-chloroform-isoamyl alcohol extraction and ethanol precipitation. The purified DNA was subjected to quantitative RT-PCR or used to construct a sequencing library by TruSeq DNA Sample Preparation Kit (Illumina) or NEBNext[®] DNA Library Prep Reagent Set (NEB) according to the manufacturer's instructions.

ChIP-Seq data processing and analysis. We mapped the reads from ChIP-Seq to the human reference genome (hg19) by BWA, retaining only unique non-duplicate reads without mismatches in the first 15 bp. Peaks were then called by MACS v1.4 (default parameter), using IgG or input as control (47). Histone modification signal is defined as the reads in one bin normalized by length of bin and total reads. The density in epigenomic modification landscapes of H3K4me3, H3K27me3 and H3K9me3 was calculated by the formula $D = Rp * 10^9 / (Rt * BL)$. Rp is the number of the unique non-duplicate reads that located in the peak regions within a bin. Rt is the total number of unique-non-duplicated ChIP-seq reads mapped to the human genome. BL is the length of a bin (bp).

Identification of “H3K9me3 mountains”. First, peaks were called by MACS with default parameters for the ChIP-Seq samples of H3K9me3 mark, using MSCs-*WRN*^{-/-} as control and MSCs-*WRN*^{+/+} as treatment. Then two neighboring peaks were merged into one peak if the distance between them was less than 2 kb. Genomic regions with peaks over 20 kb in wild-type cells were defined as “H3K9me3 mountains”. The “H3K9me3 mountains” were merged into one if the distance between them was less than 1 Mb. Only ones that were presented in both duplicates were taken into account. For the MSCs-*WRN*^{+/+} samples, we found 73 “H3K9me3 mountains”, and 48 (65.8%) of them are at sub-centromere or sub-telomere regions. 28 of “H3K9me3 mountains” were clearly lost in MSCs-*WRN*^{-/-}.

Reduced representation bisulfite sequencing (RRBS). RRBS samples were prepared as described previously (40). Briefly, for RRBS samples, 100-200 ng of genomic DNA was digested with *MspI* and purified by QIAquick PCR Purification kit (Qiagen). 50-600bp fragments were selected by 2% agarose gel. After addition of spike-in controls, samples were end-repaired, dA-tailed and ligated to methylated adapters from the TruSeq DNA Sample Preparation Kit (Illumina). The ligated DNA was then treated with bisulfite using MethylCode Kit (Invitrogen) converting unmethylated cytosine (C) into uracil (U). Finally, sequencing libraries were prepared by PCR amplification with PfuTurbo Cx Hotstart DNA polymerase (Agilent Technologies). Spike-in controls were designed as previously mentioned. The bisulfite conversion rates of the RRBS samples were 99.77% (MSCs-*WRN*^{+/+}) and 99.71% (MSCs-*WRN*^{-/-}) respectively.

RRBS data analysis. First, the raw reads were filtered to remove the reads of low quality or of adapter sequences. Then, the filtered reads without adapters and with high quality bases were mapped to the human reference genome and were analyzed by Bismark and Bowtie using default parameters (48, 49). Only the positions with coverage over 5 times were

taken into account.

RNA isolation and sequencing library construction. Total RNA was extracted from cells using the RNeasy Mini Kit (Qiagen) following the manufacturer's protocol. After total RNA was quantified by Fragment Analyzer (Advanced Analytical), 1-2 µg of total RNA was used to prepare a sequencing library using the TruSeq RNA Sample Preparation Kit (Illumina). In short, the RNA sample was treated with Elute, Prime, and Fragment Mix; afterwards the first and the second strand cDNAs were synthesized in succession. Next dA-tailing was performed on end-repaired DNA. Then adapters were ligated to the fragments. Lastly, ligated DNA fragments were enriched with 8-10 cycles of PCR.

RNA-Seq data analysis. We aligned the reads from RNA-Seq to the human reference genome (hg19 RefSeq from UCSC) by BWA and then calculated the RPKM of each gene (41-44). $RPKM = MR / (TR(\text{million}) * EL(\text{kb}))$, MR is the total number of reads that were mapped to transcripts of the gene, TR is the total number of reads that were mapped to the reference, EL is the length of the longest transcript of a gene. 14,124 and 12,295 genes with RPKM over 0.1 were detected in ESCs and MSCs, respectively. Gene Ontology (GO) for enrichment of genes was assessed with DAVID (45, 46).

Accession number. The sequencing data used in this study were deposited in the GEO database and were accessible through the accession numbers GSE52285 and SRP041072.

Statistical analysis. The statistical analyses were performed using PRISM Version 5 software (Graphpad Software). Data are presented as mean+SEM. Comparisons were performed with student's t-test or one-way anova. $P < 0.05$ was defined as statistically significant.

Supplemental Figures

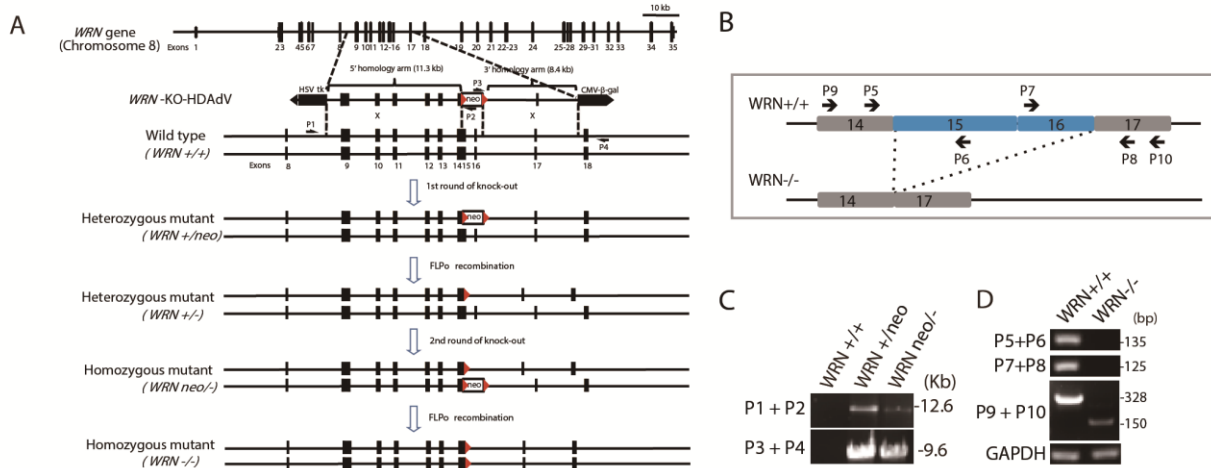


Figure S1. Generation of WRN-deficient ESCs by gene targeting. (A) Schematic representation of *WRN* targeting using *WRN*-HDAV. HSVtk stands for herpes simplex virus thymidine kinase gene cassette used for negative selection; neo stands for neomycin-resistance gene cassette used for positive selection; CMV- β -gal indicates the β -gal expression cassette for determination of HDAV titer; Red triangle, *FRT* site. (B) Schematic molecular representation of *WRN* mRNA structure. (C) PCR analyses of genomic DNAs from parental wild-type ESCs (*WRN*^{+/+}), heterozygous mutant (*WRN*^{+/neo}) and homozygous mutant (*WRN*^{neo/-}) via the 5' primer pair (P1 and P2; 12.6 kb) or the 3' primer pair (P3 and P4; 9.6 kb). (D) Analysis of *WRN* mRNA expression in ESCs-*WRN*^{+/+} and ESCs-*WRN*^{-/-} by RT-PCR with primers indicated in fig. S1B.

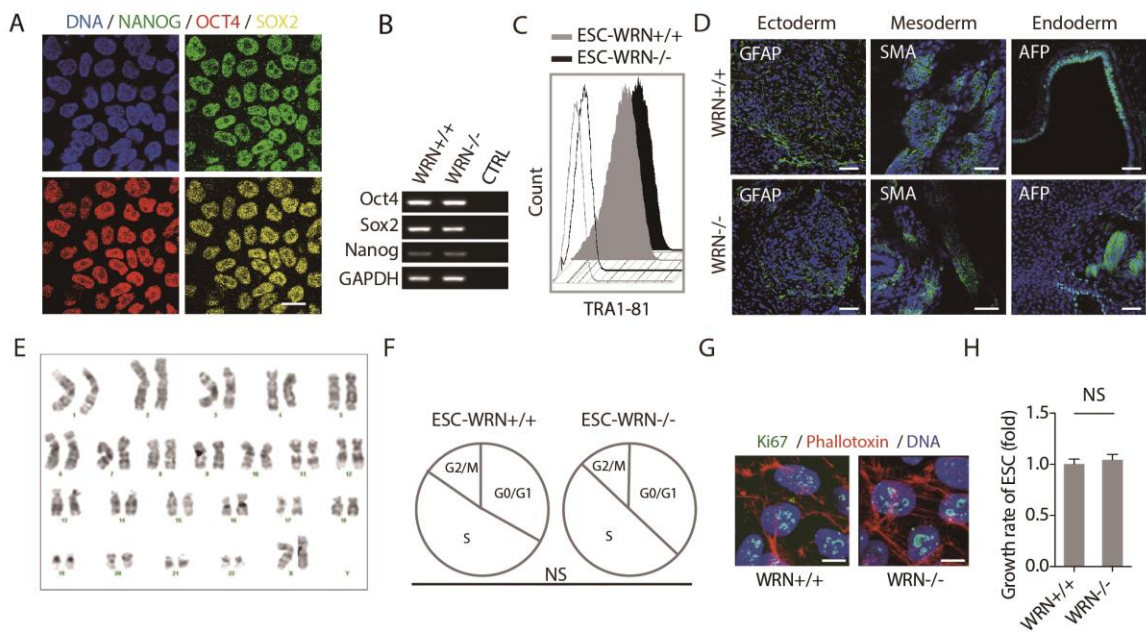


Figure S2. Characterization of WRN-deficient ESCs. (A) Immunofluorescence analyses of pluripotency markers in

ESCs-*WRN*^{-/-} (clone # 2). Scale bar, 25 μ m. **(B)** RT-PCR analyses of the expression of pluripotency markers in ESCs-*WRN*^{+/+} and ESCs-*WRN*^{-/-}. CTRL, use H₂O as template blank. **(C)** FACS analyses of the pluripotency marker TRA1-81 in ESCs-*WRN*^{+/+} and ESCs-*WRN*^{-/-}. Samples treated with or without primary antibody were represented by blank or filled curves, respectively. **(D)** Immunostaining of representative markers of the three germ layers in teratomas developed from ESCs-*WRN*^{+/+} and ESCs-*WRN*^{-/-}. Scale bar, 75 μ m. **(E)** Karyotyping analysis of P31 ESCs-*WRN*^{-/-} revealing a normal karyotype. **(F)** Cell cycle analysis showing no marked difference between ESCs-*WRN*^{+/+} and ESCs-*WRN*^{-/-}. **(G)** Immunostaining of Ki67 in ESCs-*WRN*^{+/+} and ESCs-*WRN*^{-/-}. Scale bar, 7.5 μ m. **(H)** Relative growth rates of ESCs were evaluated by cell count. Data represent mean + SEM. NS: not significant by t-test; n=3.

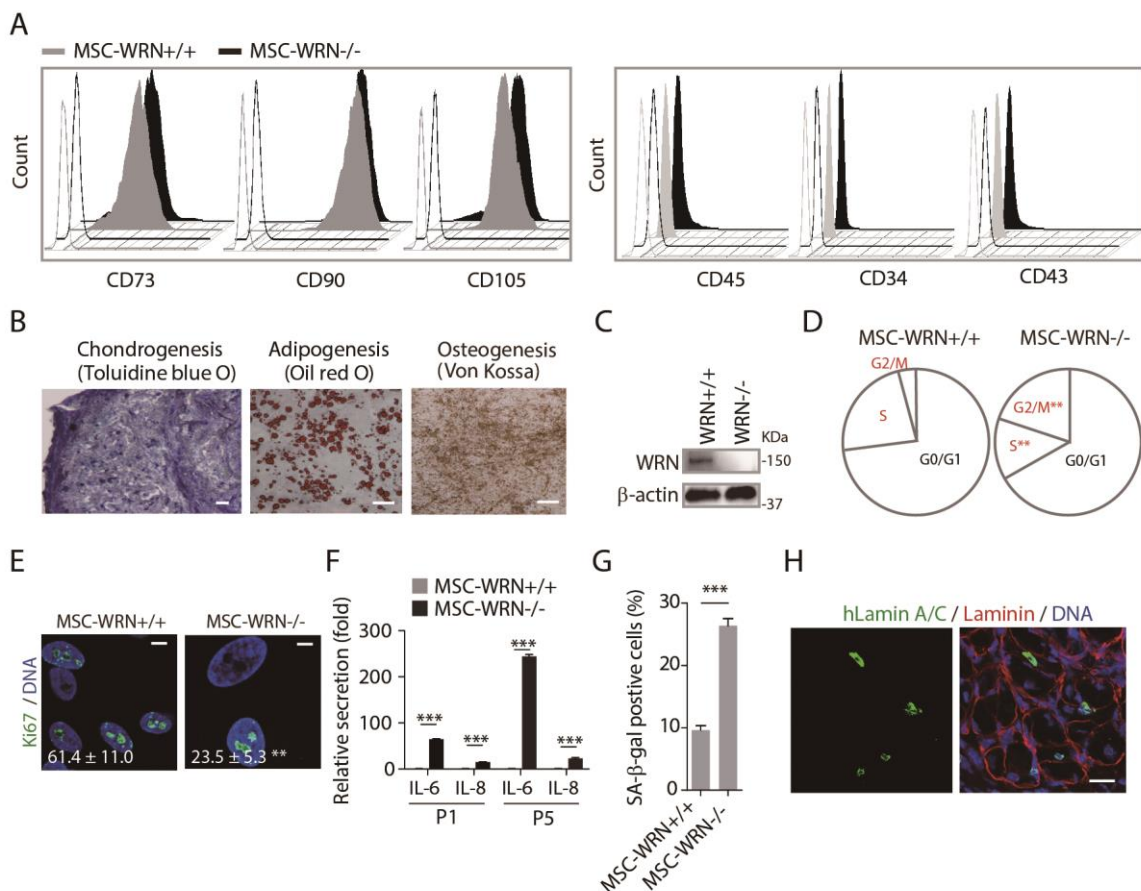


Figure S3. WRN-deficient MSCs exhibited features characteristic of accelerated cellular senescence. **(A)** FACS analysis of MSC-specific cell surface markers (CD73, CD90, and CD105) and MSC-irrelevant markers CD45, CD34, and CD43 in MSCs-*WRN*^{+/+} and MSCs-*WRN*^{-/-} at P1. **(B)** Characterization of tri-lineage differentiation potential of P5 MSCs-*WRN*^{-/-}. Toluidine blue O, oil Red O, and Von Kossa staining were used to evaluate osteogenesis, chondrogenesis, and adipogenesis potential of MSCs, respectively. Scale bar, 100 μ m. **(C)** Western blots showing the absence of WRN protein in P5 MSCs-*WRN*^{-/-}. **(D)** FACS-based cell cycle analysis of P5 MSCs showing that MSCs-*WRN*^{-/-} were arrested at G2/M phase. **(E)** Representative immunostaining images showing decreased expression

of Ki67 in P5 MSCs-WRN^{-/-}. Scale bar, 10 μ m. Percentages of Ki67-positive cells were shown on the bottom. **(F)** ELISA showing an increase in IL-6 and IL-8 secretion in MSCs-WRN^{-/-} at P1 and P5, respectively. Data were normalized to the MSCs-WRN^{+/+} group. **(G)** SA- β -gal staining of MSCs-WRN^{-/-} derived from ESCs-WRN^{-/-} (clone # 2). **(H)** Representative image of immunofluorescence showing integration of MSCs-WRN^{+/+} grafts in the skeletal muscle tissue of NOD-SCID mice 7 days after transplantation. Scale bar, 50 μ m. All data are represented as mean + SEM. **P<0.01, ***P<0.001 by t test; n=3.

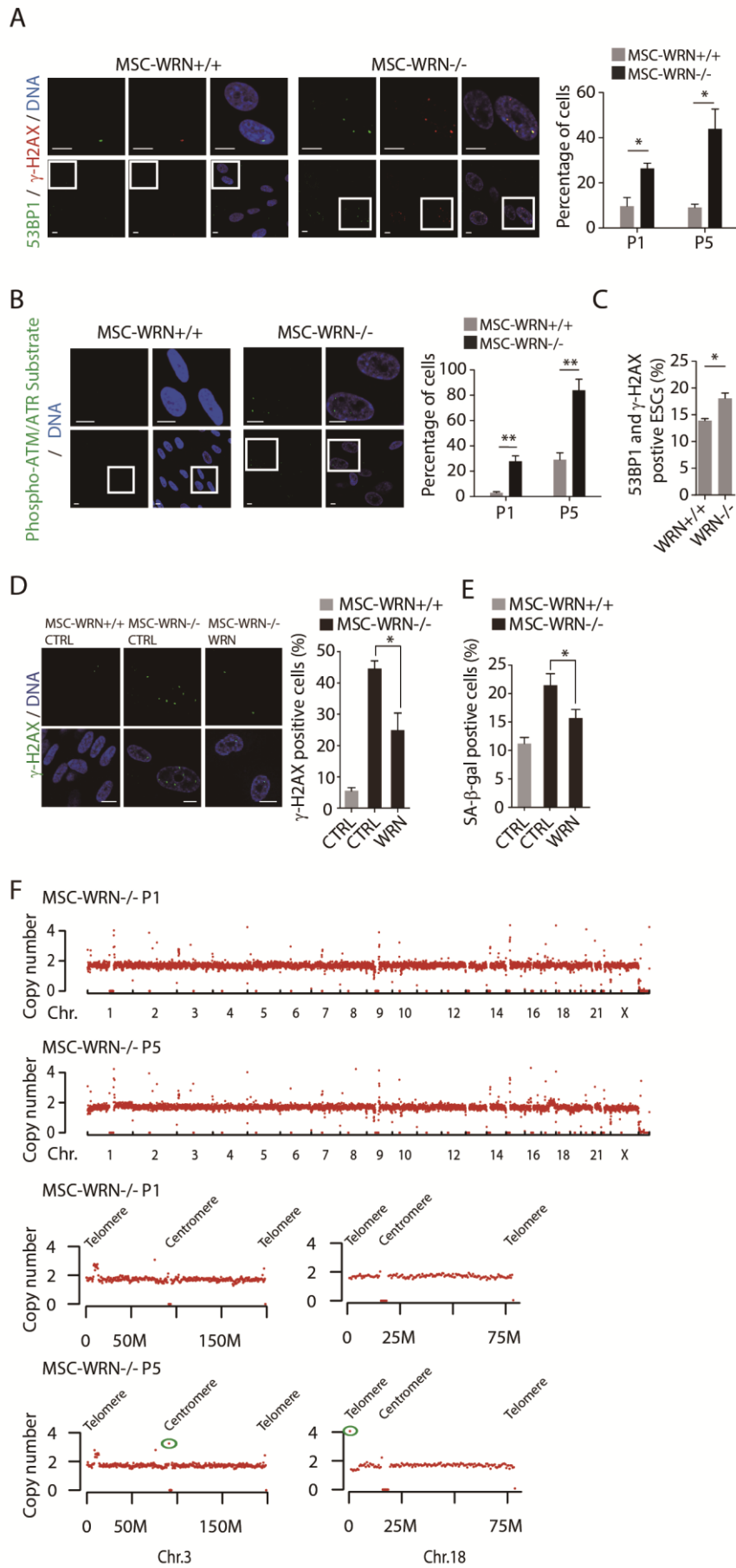


Figure S4. Deficiency of WRN in MSCs resulted in an elevated DNA damage response (DDR). (A) Left, Immunostaining of 53BP1 and γ -H2AX in P5 MSCs-*WRN*^{+/+} and MSCs-*WRN*^{-/-}. Scale bar, 10 μ m. Right, quantification of 53BP1 and γ -H2AX double positive foci in P1 and P5 MSCs. (B) Immunostaining of Phospho-(Ser/Thr) ATM/ATR Substrates (left, P5) and quantification of nuclei with positive foci (right) in P1 and P5 MSCs with the indicated genotypes. Scale bar, 10 μ m. (C) Quantification of 53BP1 and γ -H2AX double positive foci in ESCs. (D) MSCs-*WRN*^{-/-} were transduced with the lentiviral vector encoding WRN (WRN) or a control lentiviral vector (CTRL) at P3 and cultured to P5. Immunostaining of γ -H2AX (left) and quantification of γ -H2AX-positive nuclei (right) showed that WRN overexpression diminished DDR in MSCs-*WRN*^{-/-}. Scale bar, 10 μ m. (E) Quantitation of SA- β -gal staining of MSCs-*WRN*^{-/-} transduced with a lentiviral vector encoding WRN or a control lentiviral vector. (F) Whole genome sequencing analysis of copy number variations (CNVs) in P1 and P5 MSCs-*WRN*^{-/-}. Green circles indicated two small CNVs in P5 MSCs-*WRN*^{-/-} compared with P1 MSCs-*WRN*^{-/-}, which located at sub-centromeric (Chromosome 3) and sub-telomeric (Chromosome 18) regions (below). For A-D, more than 100 randomly selected nuclei were calculated for each group. All data are represented as mean + SEM. *P<0.05, **P<0.01 by t test; n=3.

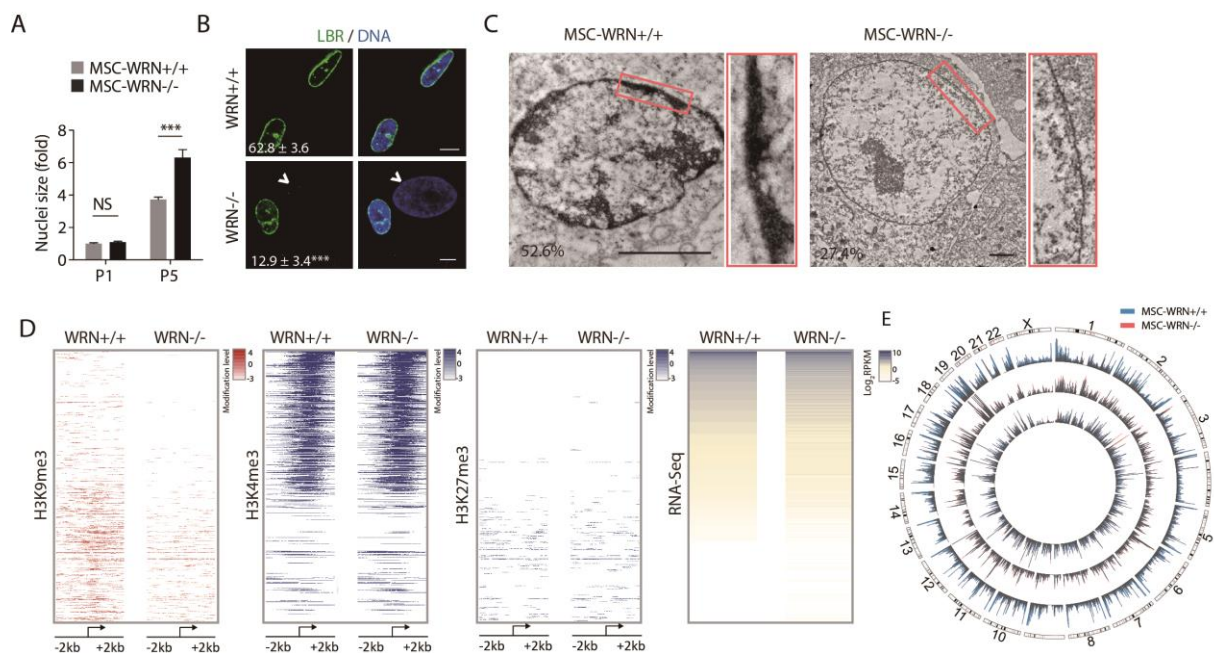


Figure S5. Nuclear architecture and epigenomic analyses of WRN-deficient MSCs. (A) Relative size of MSCs nuclei was determined at the indicated passages by Hoechst staining with ImageJ software. (B) Immunofluorescence analyses of LBR expression in MSC-*WRN*^{+/+} and MSC-*WRN*^{-/-} at P5. Arrowheads denote the abnormal nuclei with decreased LBR expression along the nuclear envelope (Percentage of LBR-positive cells presented at corner). Scale bar, 10 μ m. For A-B, more than 100 nuclei were calculated. (C) The representative EM images for MSCs-*WRN*^{+/+} and MSCs-*WRN*^{-/-} at P5 showing reduced heterochromatin architecture at the nuclear periphery in MSCs-*WRN*^{-/-}.

High-magnification view images of heterochromatin underneath nuclear envelope were shown on the right. The percentages of cells with dense heterochromatin at nuclear periphery as illustrated in the left panel were shown at the corner of each picture. Scale bar, 1 μ m. **(D)** Heatmap showing enrichment of H3K9me3, H3K4me3 and H3K27me3 at the promoter regions (-2kb to +2kb relative to the transcription start sites (TSSs)) of RefSeq genes, which were sorted by the gene expression level from high to low. **(E)** Circular map of genome-wide distribution of H3K9me3 (the outermost track), H3K4me3 (the middle track) and H3K27me3 (the innermost track) between P5 *WRN*^{+/+} and *WRN*^{-/-} in MSCs. The histone modification signal on every chromosome was visualized by Circos software (50). All data are represented as mean + SEM. ****P*<0.001, NS means not significant by t test; n=3.

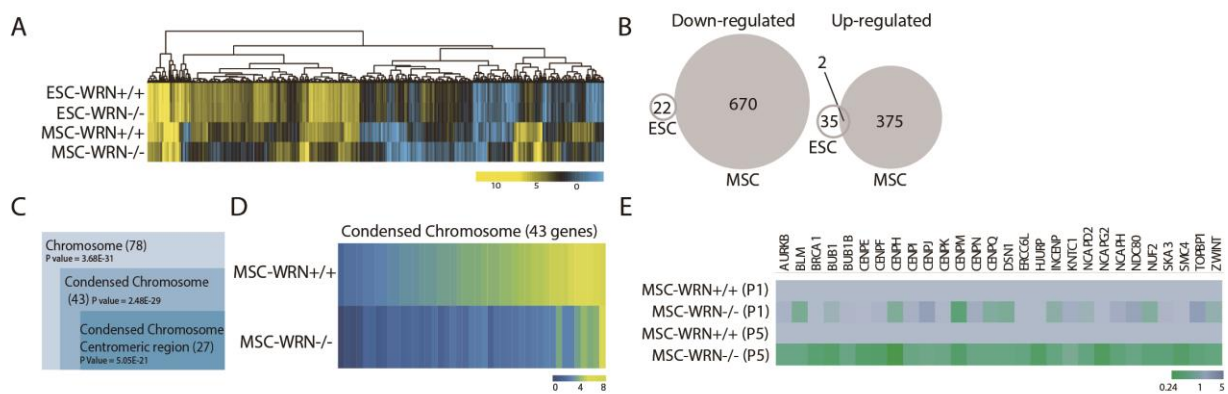


Figure S6. Transcriptomic analyses of WRN-deficient MSCs. **(A)** Heatmap showing the expression levels of the differentially expressed genes between *WRN*^{+/+} and *WRN*^{-/-} in ESCs and MSCs ($FC [WRN^{-/-} / WRN^{+/+}] >2$ or <0.5 , $p < 0.05$). **(B)** Venn diagrams showing that ESCs and MSCs share few downregulated genes ($FC [WRN^{-/-} / WRN^{+/+}] < 0.5$, $p < 0.05$, left) or upregulated genes ($FC [WRN^{-/-} / WRN^{+/+}] > 2$, $p < 0.05$, right) upon depletion of WRN. **(C)** Selected top terms from the cellular component GO analysis of downregulated genes ($FC [MSC-WRN^{-/-} / MSC-WRN^{+/+}] < 0.5$, $p < 0.05$) in P5 MSCs-*WRN*^{-/-} compared with MSCs-*WRN*^{+/+}. Gene numbers are indicated in brackets. **(D)** Heatmap showing the expression levels of the downregulated genes enriched in the GO term “condensed chromosome” between P5 MSC-*WRN*^{+/+} and MSC-*WRN*^{-/-}. **(E)** Quantitative PCR analysis of differentially expressed genes between MSCs-*WRN*^{+/+} and MSCs-*WRN*^{-/-} at P1 and P5 revealed deregulation of chromosomal condensation genes in MSCs-*WRN*^{-/-} in a passage-dependent manner. The expression level of each gene was normalized to the MSCs-*WRN*^{+/+} group. Genes with smaller mean value are color coded toward green.

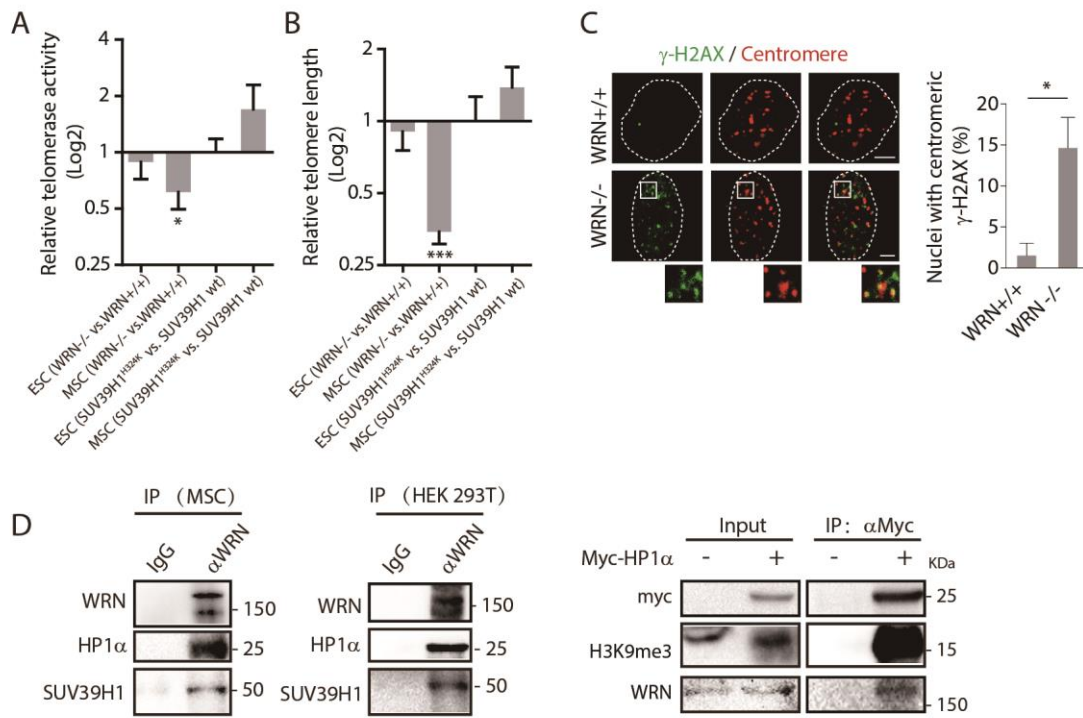


Figure S7. WRN formed complex with SUV39H1 and HP1 α . (A) TRAP assay of telomerase activity in ESCs and MSCs. Telomerase activity is assessed by the PCR amplification of telomerase products. The intensity of the products are calculated and normalized to their internal standard band after electrophoresis. (B) Relative telomere lengths were measured by quantitative real-time PCR. Genomic DNAs were isolated from ESCs and MSCs, and telomere and 36B4 primers were used to measure the relative length of telomere. (C) Left, Co-staining of centromeric DNA repeats with γ -H2AX in P5 MSCs. Representative nuclei showing double labeling by the γ -H2AX antibody (green) and centromeric FISH probe (red). The merged view shows yellow dots demonstrating DNA damage at the centromere. Scale bar, 5 μ m. Right, Quantitative analysis of the percentage of nuclei consisting of yellow dots showing significant increase of centromeric DNA damage response in MSCs-WRN^{-/-}. More than 100 nuclei were calculated for each group. (D) The presence of SUV39H1 and HP1 α proteins in anti-WRN immunoprecipitates in WRN-overexpressed primary human MSCs (left) and HEK 293T cells (middle). Right, co-immunoprecipitation of WRN and H3K9me3 with ectopically overexpressed Myc-HP1 α . All data are represented as mean + SEM. *P<0.05,***P<0.001; n=3.

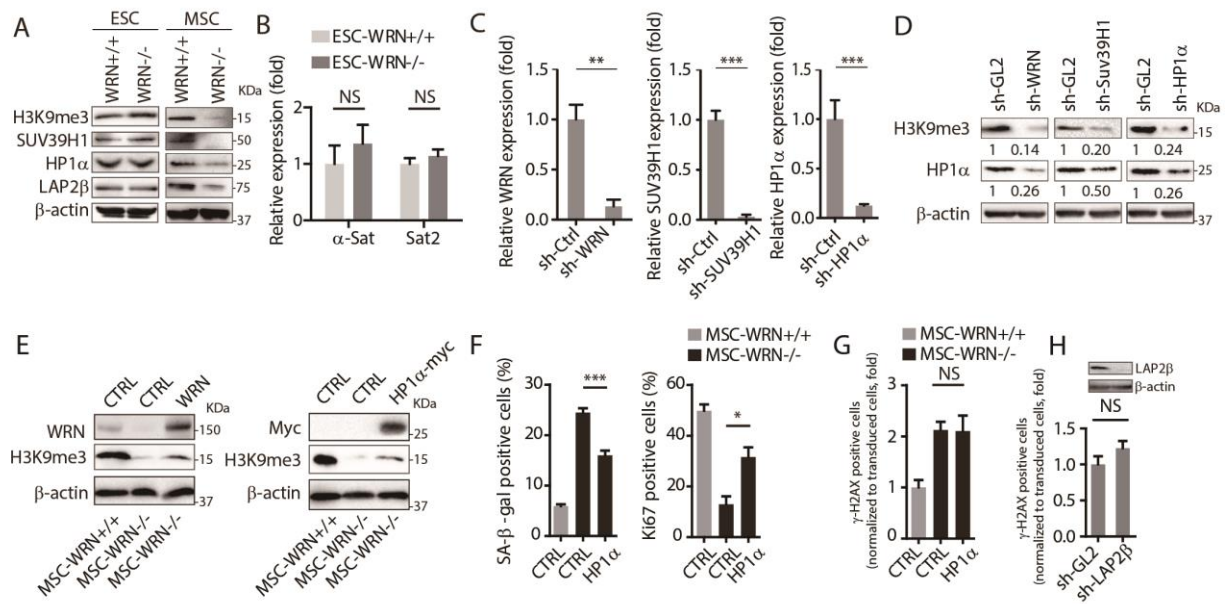


Figure S8. Heterochromatin changes contribute to accelerated senescence in WRN-deficient MSCs. (A) Western blot analysis of heterochromatin-related proteins in ESCs and P5 MSCs. (B) Quantitative RT-PCR analysis of the centromeric repetitive element transcripts in ESCs with the indicated genotypes. (C) Quantitative RT-PCR analysis of gene knock-down efficiency in human primary MSCs transduced with WRN, SUV39H1 or HP1 α -specific shRNA. (D) H3K9me3 and HP1 α levels in P5 wild-type MSCs transduced with a control lentiviral vector (sh-GL2) or a lentiviral vector encoding for the indicated shRNA. (E) MSCs-*WRN*^{-/-} were transduced with the lentiviral vector encoding WRN (WRN), HP1 α -myc, or a control lentiviral vector (CTRL) at P3 and cultured to P5, and H3K9me3 levels were determined by Western blot analysis. (F) SA- β -gal staining (left) and Ki67 staining (right) analyses in wild-type MSCs or WRN-deficient MSCs transduced with a control lentiviral vector (CTRL) or lentiviral vectors expressing HP1 α -myc. (G) Quantification of γ -H2AX-positive nuclei showing that HP1 α overexpression did not diminish DNA damage response in MSCs-*WRN*^{-/-}. (H) Quantification of nuclei with γ -H2AX foci in wild-type MSCs transduced with a control lentiviral vector (sh-GL2) or lentiviral vectors encoding for the LAP2 β shRNA. Knockdown of LAP2 β in wild-type MSCs did not significantly elevate γ -H2AX foci. All data are represented as mean + SEM. **P*<0.05, ***P*<0.01, ****P*<0.001, and NS means not significant by t test; *n*=3.

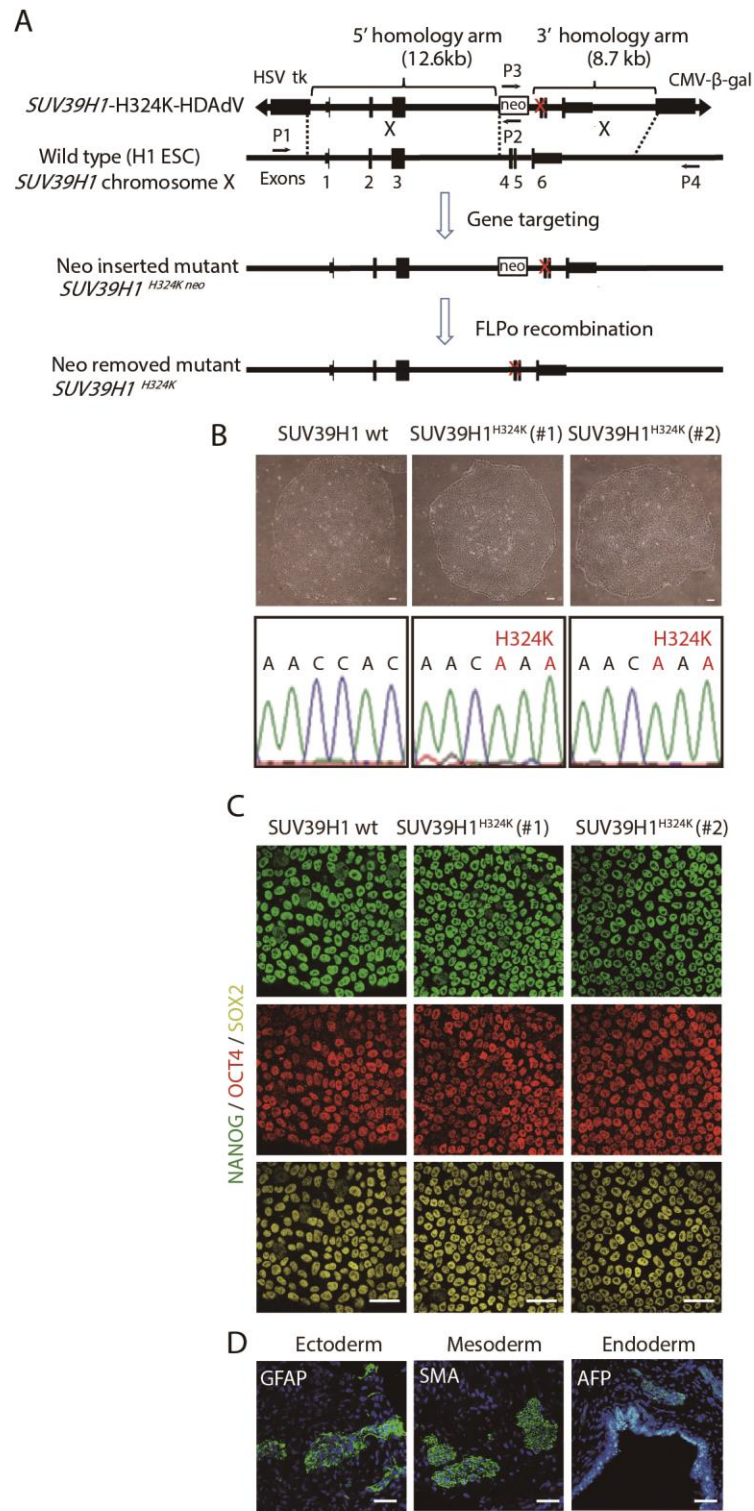


Figure S9. Characterization of ESCs-*SUV39H1*^{H324K}. (A) Schematic molecular representation of *SUV39H1*^{H324K} targeting strategy. (B) Morphological and genotypic characterization of ESCs-*SUV39H1*^{H324K}. Scale bar, 50µm. (C) Immunofluorescence showing the expression of ESC-specific markers in *SUV39H1* wild-type (wt) and H324K mutant ESCs. Scale bar, 25 µm. (D) Immunostaining of representative markers of the three germ layers in teratomas developed from *SUV39H1*^{H324K} mutant ESCs. Scale bar, 50 µm.

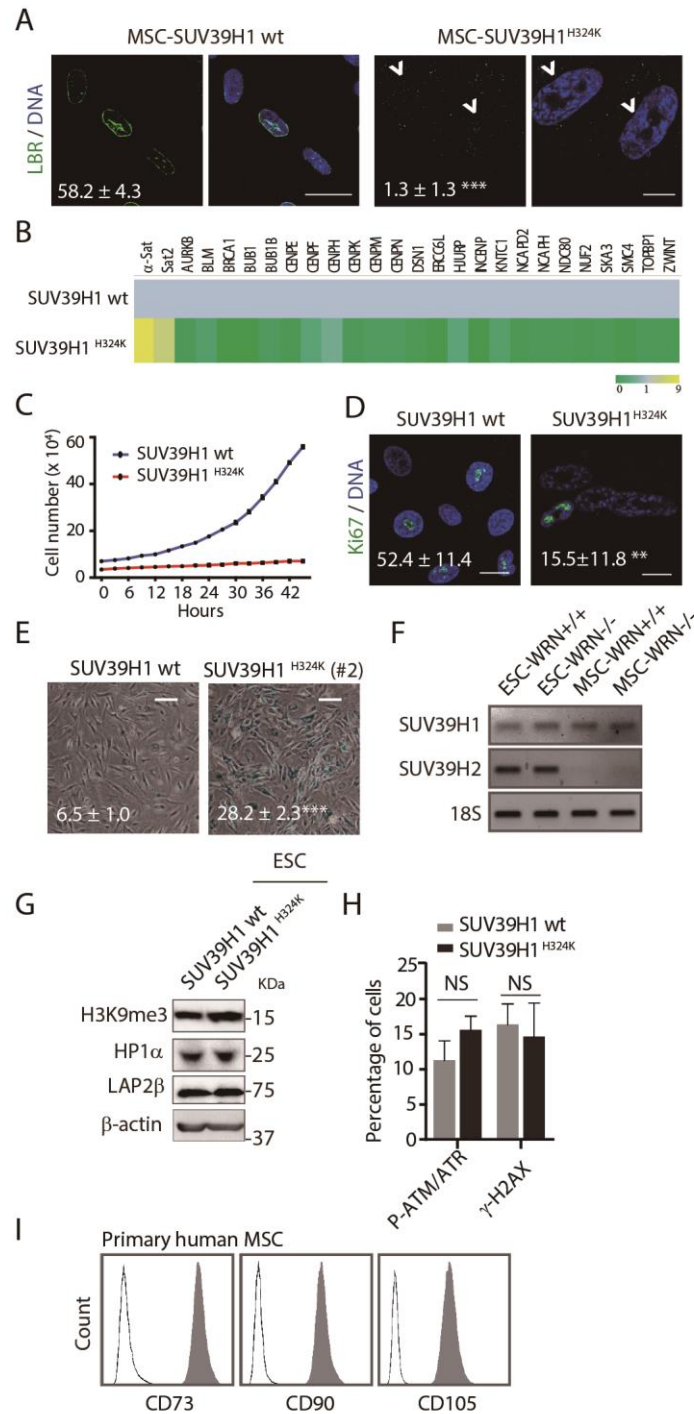


Figure S10. Heterochromatin changes as a driver for MSC aging. (A) Disorganization of nuclear lamina in *SUV39H1*^{H324K} MSCs. Immunofluorescence analyses of LBR expression in MSCs-*SUV39H1* wt and MSCs-*SUV39H1*^{H324K}. Arrowheads denote the abnormal nuclei with decreased LBR expression along the nuclear envelope (percentages of LBR-positive cells presented at corner). Scale bar, 20 μm. (B) Quantitative PCR analysis of differentially expressed genes between MSCs-*SUV39H1* wt and MSCs-*SUV39H1*^{H324K} indicates upregulation of centromeric satellite DNA expression and downregulation of transcripts encoding for chromosomal condensation proteins. The transcript levels in MSCs-*SUV39H1* wt group were normalized to one. (C) Live cell imaging recording of

cell proliferation kinetics of MSCs-*SUV39H1* wt and MSCs-*SUV39H1*^{H324K} at P5. The first record started at 12 hours after seeding. (D) Ki67 immunostaining in MSCs-*SUV39H1* wt and MSCs-*SUV39H1*^{H324K} at P5. Percentage of Ki67+ cells are presented at corner. (E) SA-β-gal staining in MSCs-*SUV39H1* wt and another line (#2) of MSCs-*SUV39H1*^{H324K}. Scale bar, 50μm. Percentages were presented on the bottom. (F) RT-PCR analyses of *SUV39H1* and *SUV39H2* in ESCs and MSCs with the indicated genotypes. (G) Western blot analysis of heterochromatin marks in ESCs. (H) Quantification of nuclei with γ-H2AX or Phospho-(Ser/Thr) ATM/ATR Substrates positive foci in MSCs with the indicated genotypes. All data are represented as mean + SEM. NS means not significant by t test; n=3. (I) FACS analysis of MSC-specific cell surface markers (CD73, CD90, and CD105) in human dental tissue-derived primary MSCs.

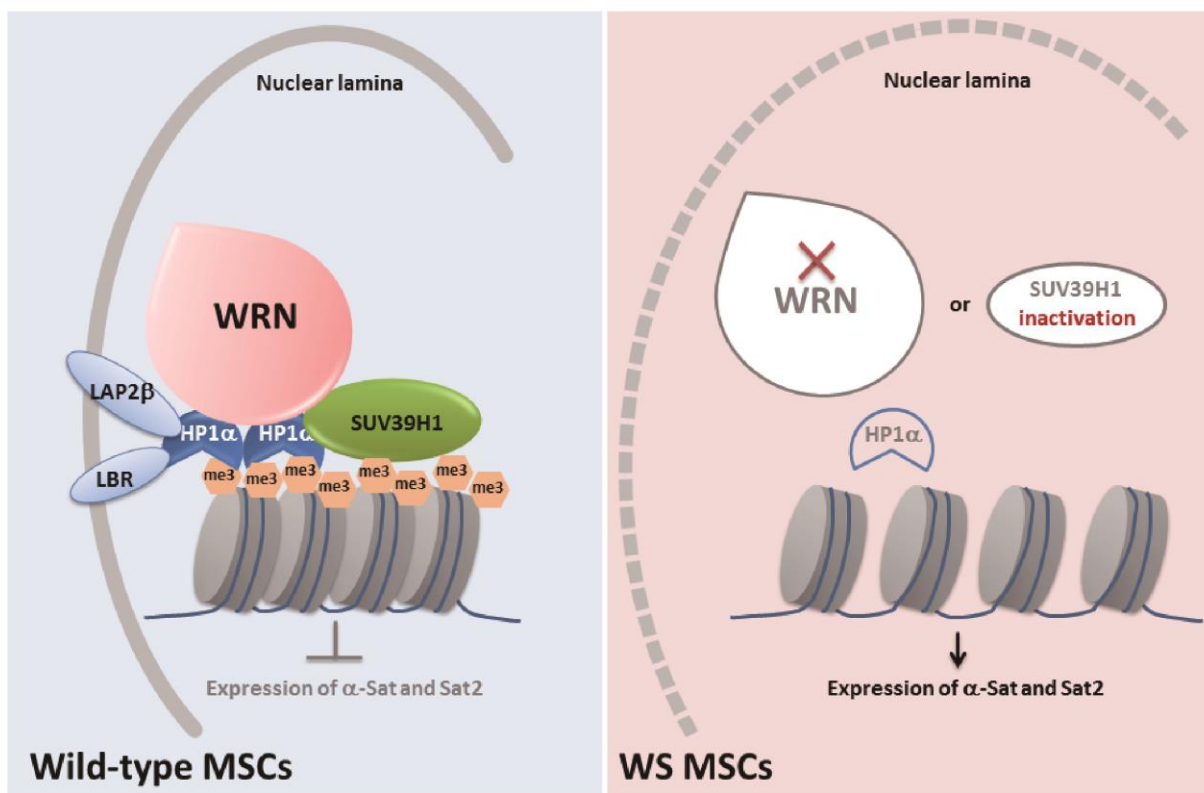


Figure S11. A proposed model describing a role of WRN in safeguarding heterochromatin stability. Left, in wild-type MSCs, WRN protein forms a complex with the heterochromatin components *SUV39H1* and *HP1α*, which together associates with H3K9me3-enriched heterochromatin tethered to nuclear envelope regions. Right, the complex was destroyed with WRN loss or *SUV39H1* inactivation, which resulted in destabilization of heterochromatin, disorganization of nuclear lamina, and induced transcription from centromeric α -Sat and Sat2 sequences, which may collectively drive premature MSC aging.

Supplemental Table Legend

Table S1. List of “H3K9me3 mountains” in MSCs-*WRN*^{+/+}

Table S2. List of differentially expressed genes (fold change, FC [*WRN*^{-/-}/*WRN*^{+/+}] > 2 or < 0.5, p<0.05) between *WRN*-proficient and *WRN*-deficient ESCs and MSCs.

Table S3. Gene ontology analysis of differentially expressed genes (fold change, FC [MSC-*WRN*^{-/-}/ MSC-*WRN*^{+/+}] > 2 or < 0.5, p<0.05) between MSCs-*WRN*^{+/+} and MSCs-*WRN*^{-/-}.

Table S4. Information on dental pulp-derived primary MSCs

Table S5. Primers list

REFERENCES

21. B. Li, S. P. Jog, S. Reddy, L. Comai, WRN controls formation of extrachromosomal telomeric circles and is required for TRF2DeltaB-mediated telomere shortening. *Mol Cell Biol* **28**, 1892 (Mar, 2008).
22. S. Lachapelle *et al.*, Proteome-wide identification of WRN-interacting proteins in untreated and nuclease-treated samples. *Journal of proteome research* **10**, 1216 (Mar 4, 2011).
23. D. Wang *et al.*, Methylation of SUV39H1 by SET7/9 results in heterochromatin relaxation and genome instability. *Proceedings of the National Academy of Sciences of the United States of America* **110**, 5516 (Apr 2, 2013).
24. K. A. Datsenko, B. L. Wanner, One-step inactivation of chromosomal genes in Escherichia coli K-12 using PCR products. *Proc Natl Acad Sci U S A* **97**, 6640 (Jun 6, 2000).
25. K. Suzuki *et al.*, Highly efficient transient gene expression and gene targeting in primate embryonic stem cells with helper-dependent adenoviral vectors. *Proc Natl Acad Sci U S A* **105**, 13781 (Sep 16, 2008).
26. D. J. Palmer, P. Ng, Physical and infectious titers of helper-dependent adenoviral vectors: a method of direct comparison to the adenovirus reference material. *Mol Ther* **10**, 792 (Oct, 2004).
27. D. M. Shayakhmetov *et al.*, Genome size and structure determine efficiency of postinternalization steps and gene transfer of capsid-modified adenovirus vectors in a cell-type-specific manner. *J Virol* **78**, 10009 (Sep, 2004).
28. G. H. Liu *et al.*, Progressive degeneration of human neural stem cells caused by pathogenic LRRK2. *Nature* **491**, 603 (Nov 22, 2012).
29. G. H. Liu *et al.*, Modelling Fanconi anemia pathogenesis and therapeutics using integration-free patient-derived iPSCs. *Nat Commun* **5**, 4330 (2014).
30. T. Ahfeldt *et al.*, Programming human pluripotent stem cells into white and brown adipocytes. *Nat Cell Biol* **14**, 209 (Feb, 2012).
31. D. R. Deyle *et al.*, Normal collagen and bone production by gene-targeted human osteogenesis imperfecta iPSCs. *Mol Ther* **20**, 204 (Jan, 2012).
32. S. Kaitainen *et al.*, TiO₂ coating promotes human mesenchymal stem cell proliferation without the loss of their capacity for chondrogenic differentiation. *Biofabrication* **5**, 025009 (Jun, 2013).
33. G. T. Huang, S. Gronthos, S. Shi, Mesenchymal stem cells derived from dental tissues vs. those from other sources: their biology and role in regenerative medicine. *J Dent Res* **88**, 792 (Sep, 2009).
34. L. Pierdomenico *et al.*, Multipotent mesenchymal stem cells with immunosuppressive activity can be easily isolated from dental pulp. *Transplantation* **80**, 836 (Sep 27, 2005).
35. X. Chen *et al.*, Quantitative proteomics analysis identifies mitochondria as therapeutic targets of multidrug-resistance in ovarian cancer. *Theranostics* **4**, 1164 (2014).
36. F. Debacq-Chainiaux, J. D. Erusalimsky, J. Campisi, O. Toussaint, Protocols to detect senescence-associated beta-galactosidase (SA-betaGal) activity, a biomarker of senescent cells in culture and in vivo. *Nat Protoc* **4**, 1798 (2009).
37. A. Freund, C. K. Patil, J. Campisi, p38MAPK is a novel DNA damage response-independent regulator of the senescence-associated secretory phenotype. *Embo J* **30**, 1536 (Apr 20, 2011).
38. R. M. Cawthon, Telomere measurement by quantitative PCR. *Nucleic Acids Res* **30**, e47 (May 15, 2002).
39. J. A. Dahl, P. Collas, A rapid micro chromatin immunoprecipitation assay (microChIP). *Nat Protoc* **3**, 1032 (2008).
40. L. Wen *et al.*, Whole-genome analysis of 5-hydroxymethylcytosine and 5-methylcytosine at base resolution in the human brain. *Genome Biol* **15**, R49 (Mar 4, 2014).
41. L. R. Meyer *et al.*, The UCSC Genome Browser database: extensions and updates 2013. *Nucleic Acids Res* **41**, D64 (Jan, 2013).

42. D. Karolchik *et al.*, The UCSC Table Browser data retrieval tool. *Nucleic Acids Res* **32**, D493 (Jan 1, 2004).
43. H. Li, R. Durbin, Fast and accurate long-read alignment with Burrows-Wheeler transform. *Bioinformatics* **26**, 589 (Mar 1, 2010).
44. E. S. Lander *et al.*, Initial sequencing and analysis of the human genome. *Nature* **409**, 860 (Feb 15, 2001).
45. W. Huang da, B. T. Sherman, R. A. Lempicki, Systematic and integrative analysis of large gene lists using DAVID bioinformatics resources. *Nat Protoc* **4**, 44 (2009).
46. W. Huang da, B. T. Sherman, R. A. Lempicki, Bioinformatics enrichment tools: paths toward the comprehensive functional analysis of large gene lists. *Nucleic Acids Res* **37**, 1 (Jan, 2009).
47. Y. Zhang *et al.*, Model-based analysis of ChIP-Seq (MACS). *Genome Biol* **9**, R137 (2008).
48. F. Krueger, S. R. Andrews, Bismark: a flexible aligner and methylation caller for Bisulfite-Seq applications. *Bioinformatics* **27**, 1571 (Jun 1, 2011).
49. B. Langmead, C. Trapnell, M. Pop, S. L. Salzberg, Ultrafast and memory-efficient alignment of short DNA sequences to the human genome. *Genome Biol* **10**, R25 (2009).
50. M. Krzywinski *et al.*, Circos: an information aesthetic for comparative genomics. *Genome Res* **19**, 1639 (Sep, 2009).